Construction and Building Materials 489 (2025) 142379

Contents lists available at ScienceDirect

Construction and Building Materials

journal homepage: www.elsevier.com/locate/conbuildmat

Effects of hazardous spills by road accidents on pavement texture and its deterioration mechanism

Zhenlong Gong [a,b], Marco Bruno [b,*], Claudio Lantieri [b], Margherita Pazzini [b], Yinghao Miao [a,*]

[a] National Center for Materials Service Safety, University of Science and Technology Beijing, Beijing, China
[b] Dicam - Department of Civil, Chemical, Environmental and Material Engineering, University of Bologna, Italy

ARTICLE INFO

Keywords:
Road safety
Hazardous spills
Pavement texture
Skid resistance
Close-range photogrammetry
Molecular dynamics
Road deterioration mechanism

ABSTRACT

Hazardous spills from road accidents affect road safety, reduce the skid resistance of pavement and have a long-term impact on pavement texture. This paper conducted experimental investigation and molecular dynamics simulations on common road accident hazardous spills (petrol, diesel, engine oil, and brake fluid). A low-cost close-range photogrammetry technique was used to measure changes in pavement texture. The texture wear process of the contaminated pavement was simulated by using the Hamburg Wheel Tracking Device. Material Studio was used to simulate the interaction between hazardous spills and the bituminous conglomerate. Results showed an average reduction of 47 % in terms of skid resistance after contamination, with an absolute maximum decrease of 71 % observed with engine oil spillage. While cleaning can partially restore skid resistance, effects of contamination vary by spill type. Petrol and diesel dissolve bitumen, weakening the pavement structure, whereas engine oil remains on the surface, posing prolonged safety risks. Brake fluid infiltrates aggregates, potentially affecting their mechanical properties. The correlation between texture parameters and skid resistance is weak on newly paved roads but become more pronounced as wear progresses. Simulations reveal that hazardous spills adhere readily to bitumen and aggregates, exacerbating contamination effects. These findings provide scientific insights for optimizing spill response strategies and improving road safety management.

1. Introduction

As the number of vehicles on the road continues to increase, traffic accidents have become more frequent [1,2]. Globally, road traffic injuries have emerged as the eighth leading cause of death, contributing to substantial property damage as well as environmental and pavement-related challenges [3–6]. A particular concern is related to the hazardous substances, such as diesel, petrol, engine oil, and brake fluid, that may be released from vehicles upon collision. If the accident involves vehicles transporting these liquids, the volume of the spill is inevitably large [7–9]. Once spilled, these substances not only contaminate the environment but also significantly alter the physical and chemical properties of the pavement, diminishing skid resistance and thereby increasing the risk of secondary accidents and endangering road users' safety. [9,10]. When hazardous spills come into contact with the asphalt concrete, these liquids rapidly spread and infiltrate the surface material, causing changes to the pavement performance [11,12]. On a first impact, the spilled substances alter the skid resistance of bituminous mixture, modify the road texture and reduce the tire-pavement contact [13]. Such changes not only impair vehicle handling but may also lead to additional accidents. Over time, the infiltration of contamination causes long-term damage to the road materials, accelerating the wear of surface texture and continuously diminishing the pavement's skid resistance [14]. Therefore, accurately monitoring and assessing the changes in pavement texture following hazardous spills are of critical importance for both traffic safety and road maintenance.

Previous researches have primarily focused on analyzing the relationship between pavement texture and skid resistance, as well as the deterioration of the road surface texture under normal conditions [15–17]. Researchers generally agree that skid resistance is determined by the interaction forces between the tire and the pavement, which consist of four main factors: intermolecular forces, adhesion between the tire and the pavement, the hysteresis effect caused by internal friction and energy dissipation in the tire rubber, and the micro-cutting effect of

* Corresponding authors.
E-mail addresses: marco.bruno14@unibo.it (M. Bruno), miaoyinghao@ustb.edu.cn (Y. Miao).

https://doi.org/10.1016/j.conbuildmat.2025.142379
Received 18 March 2025; Received in revised form 5 June 2025; Accepted 20 June 2025

small micro-convexities on the pavement surface [18–21]. Therefore, automotive professionals primarily improve the friction between tires and pavement by adjusting tire tread patterns and rubber properties [22]. While road pavement engineering researchers typically focus on asphalt concrete texture roughness [23,24]. Cui et al. [25] found through their research that steel slag exhibits a more irregular surface, making the road surface layer texture rougher and enhancing skid resistance. Huan et al. [26] simulated changes in pavement texture and skid resistance due to traffic wear using a polishing device. Their study revealed that pavements exhibiting minimal texture wear produced higher levels of skid resistance. The degradation of texture is related to the abrasion resistance of the aggregate. Although it is recognized that pavement texture and its degradation are related to skid resistance, few have considered the effect of hazardous spills on this.

Some studies have considered the effect of environmental factors on pavement texture or skid resistance. Common road conditions, such as rainy and snowy weather, icy surfaces, and the presence of gravel on the road surface, have all attracted attention. Pérez-Fortes et al. [27] compared the long-term effects of normal weather with those of extreme high and low temperatures on pavement micro-textures. Their study found that normal weather had almost no impact on the microstructure of the aggregate, whereas extreme seasonal conditions caused the roughness of the aggregate to decrease by half. Gerthoffert et al. [28] developed a tire-pavement skid resistance model, introducing the concept of contaminants, but their analysis mainly focused on the change of friction during rain or snow. Hichri et al. [29] conducted experiments and modeling to analyze the effect of fine aggregates on skid resistance, finding that quartz gravel can cause variations in skid resistance test results.

These studies demonstrate that environmental factors directly impact the skid resistance performance of pavement texture and its long-term evolution. However, hazardous spills on road surfaces inevitably affect the process of texture deterioration, yet research on the effects of hazardous spills on pavements is still limited. Lantieri et al. [12] are among the few researchers who have attempted to analyze the effects of hazardous spills on skid resistance. Their tests showed that substances such as diesel and brake fluid significantly reduce skid resistance and also weaken the mechanical strength of the pavement. Although they focused on changes in skid resistance, they did not analyze the long-term and short-term effects of these spills on the pavement texture. Hazardous spills typically adhere to the pavement surface, with the most immediate effect being a reduction in skid resistance. Hazardous spills initially reduce the skid resistance of the texture, and over time these spills can also affect the degradation of the pavement texture, all of which require further study.

To address the gaps in the above research, the primary objective of this study is to investigate the short-term and long-term effects of hazardous spills from road accidents on pavement texture and to clarify the mechanism of pavement texture deterioration. A comparative analysis of the long-term texture changes due to spills such as petrol, diesel, and engine oil is conducted. Molecular dynamics simulations are used to analyze the interactions between different spills and bitumen as well as aggregates. This research provides insights into the effects of hazardous spills on pavements and offers theoretical guidance on how to reduce the impact of hazardous spills in road accidents and maintain skid resistance.

2. Materials and methodologies

2.1. Raw materials

2.1.1. Hazardous spills

Severe traffic accidents are often accompanied by the leakage of hazardous substances, which can impact pavement performance. In accidents involving fuel tankers transporting petrol or diesel, large volumes of spilled liquid can cover tens of meters of roadway, further which can have an even greater impact on the pavement [30]. Therefore, it is essential to conduct experimental research on the effects of hazardous spills. This study utilized common hazardous spills, including diesel, petrol, engine oil, and brake fluid. The relevant properties of these hazardous spill materials are presented in Table 1, which provides an overview of their key characteristics and potential interactions with pavement surfaces.

Table 1
The basic properties of hazardous spill substances.

Type	Main Components	Density range ($g \cdot cm^{-3}$)	Hydrophilicity	Characteristics
Diesel	Alkanes (C_4-C_{12}); Cycloalkanes; Aromatics	0.82–0.87	Low	Higher energy density, difficult to clean, easy to form oil film
Petrol	Alkanes(C_{12}-C_{20}); Aromatics; Polycyclic Aromatic Hydrocarbons	0.70–0.78	Low	Highly volatile, burns quickly, relatively easy to clean
Engine Oil	Semi-synthetic oils	0.85–0.95	Very low	Sticky and leaves dirt easily
Brake Fluid	Glycol ethers; Borate esters	1.02–1.09	Medium	Water washable, may leave residues

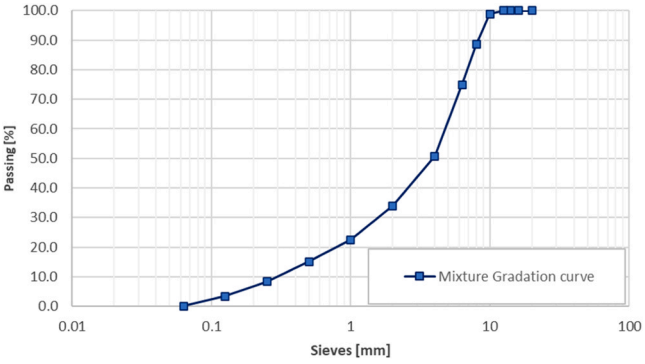

Fig. 1. Mixture gradation curve.

Table 2
Mixture characteristics and volumetric properties.

Bitumen Content (%)	[EN 12697–1]	On Aggregate On conglomerate	5.74 6.09
Aggregates Bulk Density(g/cm^3)	[EN 12697–6]		2.622
Mixture Maximum Density (g/cm^3)	[EN 12697–5]		2.394
Voids Content (%)	[EN 12697–8]		4.14

2.1.2. Pavement materials

In this study, the same asphalt mixture was used for both field and laboratory tests. This hot-mix asphalt was specifically designed for surface wear layers. Fig. 1 shows the gradation curve of the mixture employed in both settings, while in Table 2 the volumetric properties of the mixture are presented.

The mixture was prepared using conventional 50/70 bitumen, which is commonly used in urban and local road applications. The compaction temperature was set at 165°C for both laboratory and field applications. In the field trial, the ambient temperature was 15°C. The hot mix asphalt mixture was produced in a nearby plant and then transported to the test site for placement. The field application involved laying a 5 cm-thick asphalt layer over a pre-existing pavement, covering an area of 20 m in length and 4 m in width.

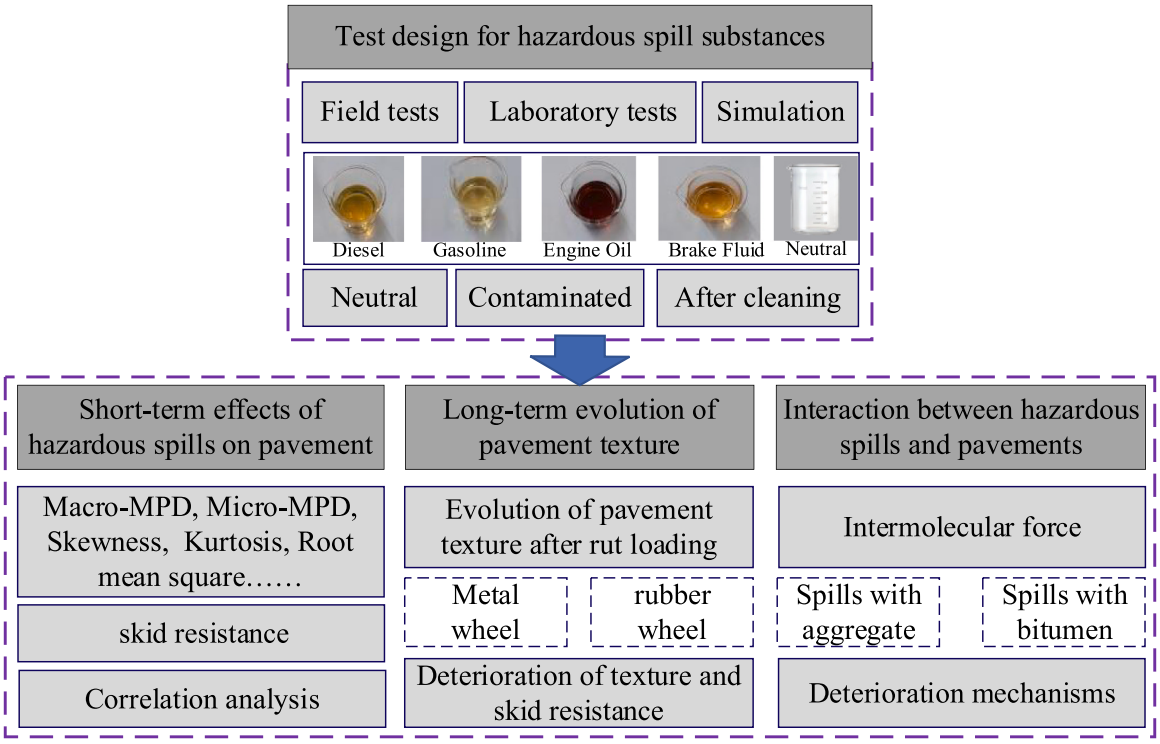

Fig. 2. The flow diagram of this study.

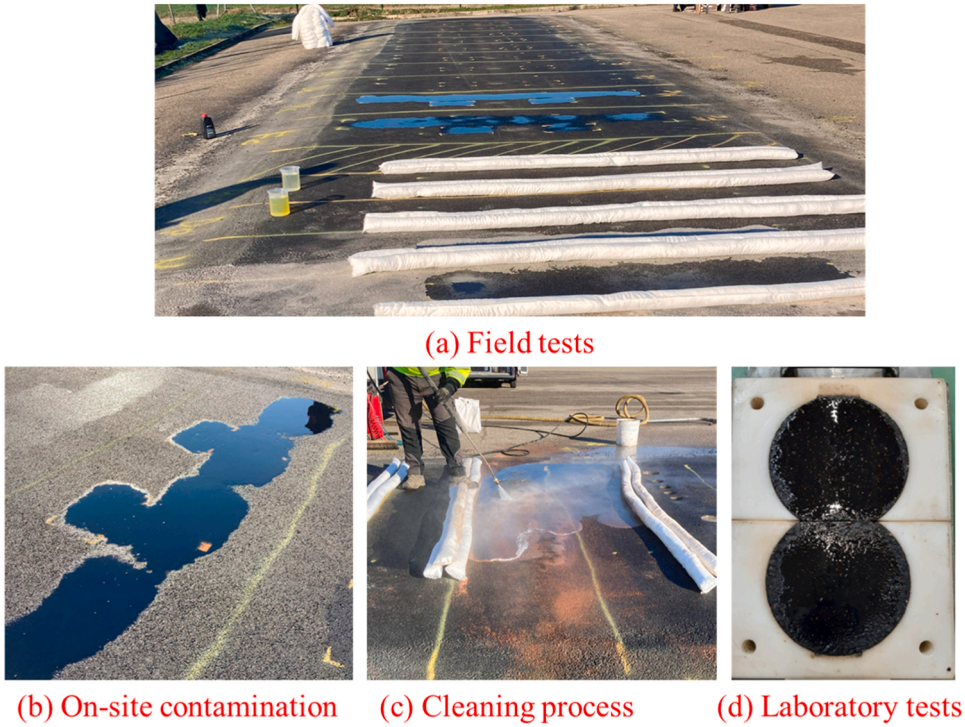

Fig. 3. Diagrams of field tests and laboratory tests.

Laboratory specimens were fabricated using a gyratory compactor, applying 110 gyrations to produce cylindrical samples with a diameter of 150 mm. To meet the dimensional requirements of the Hamburg Wheel Tracking (HWT) test mold, the specimens were subsequently cut to a final height of 6 cm.

2.2. Experimental methods

The experimental program of this study is illustrated in Fig. 2. First of all, common hazardous spills that may leak after traffic accidents were selected for both the field and the laboratory tests. The effects on the road pavements surface of petrol, diesel, engine oil and brake fluid were investigated. Pavement texture reconstruction techniques are employed

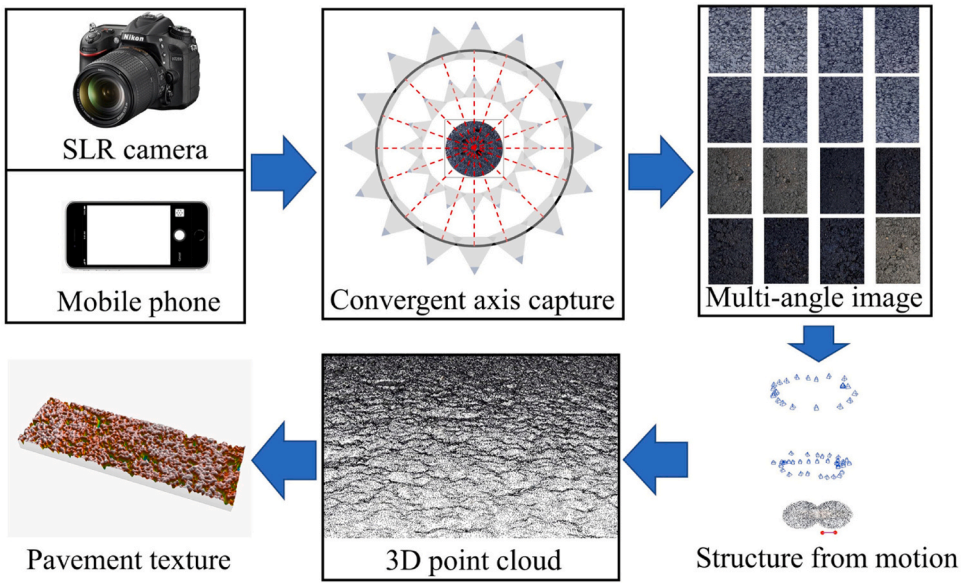

Fig. 4. Schematic diagram of pavement texture acquisition process.

to collect data and evaluate surface texture characteristics. The British Pendulum Test is conducted to measure the pavement friction coefficient and assess skid resistance. The evolution of pavement texture and skid resistance under hazardous spill contamination is investigated through rut loading simulations with Hamburg Wheel Tracking Device. Additionally, molecular dynamics (MD) simulations are used to model the interactions between various hazardous substances and both aggregates and bitumen. Based on these analyses, a deterioration mechanism of pavement texture induced by hazardous spills is proposed.

2.2.1. *Pavement contamination test design*

Both field and laboratory tests were conducted to evaluate the effects of hazardous spills on pavement surfaces as shown in Fig. 3. The field tests focused on the short-term impacts. To achieve this, a newly paved test section was divided into two groups, each consisting of five areas. One group after being contaminated was left untreated, while the other was subjected to rapid cleaning after being contaminated with petrol, diesel, engine oil, and brake fluid, respectively. Each road surface was contaminated with each pollutant according to this ratio: 0.4lt/m^2, under ambient environmental conditions of 15°C and no humidity. Cleaning procedures were initiated 30 min after the hazardous spill contamination. The process, commonly used in this case [12,30], involved four sequential steps: first, the application of a powdered calcinated clay absorbent to soak up the spilled substances; second, the mechanical removal of the absorbent material; third, washing the surface with a mixture of water and a specialized detergent; and finally, high pressure water cleaning and vacuum of the road surface.

The laboratory tests were aimed at assessing the long-term changes in pavement texture. Different types of contamination were then applied to the surface of the specimens to simulate pavement exposure to hazardous spills. The pollutants application rate used in the laboratory was consistent with that of the field trial, corresponding to approximately 4.0 lt/m^2. As in the field test, a waiting period of 30 min was observed before performing the measurements. Unlike the field procedure, the contaminated laboratory specimens were not subjected to any cleaning treatment. Nevertheless, cleaned cores extracted from the field trial were tested to evaluate the effectiveness of the cleaning procedures.

2.2.2. *Texture characterization tests*

Close-range photogrammetry (CRP) is a technique that reconstructs the 3D shape and structure of an object by capturing multiple photographs from different angles. The quality of the reconstruction depends

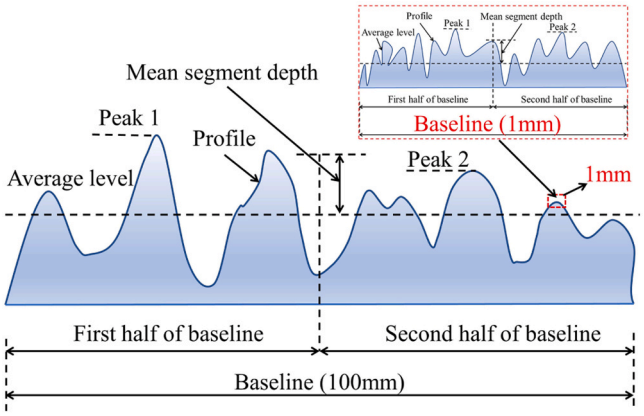

Fig. 5. Schematic of macro-MPD and micro-MPD calculation.

on factors such as image resolution, capture strategy, and the reconstruction algorithm. Images were collected using both a smartphone and a SLR camera. When using the smartphone, a convergent axis capture strategy was employed (a detailed explanation can be found in [31]). The Structure from Motion (SfM) algorithm was applied to reconstruct the pavement texture. After reconstruction, a sparse point cloud was generated. Through parallax calculation and depth estimation, the detailed geometric structure of the 3D scene was recovered from the multi-view images. The final output was a high-precision 3D point cloud, which was used to calculate the pavement texture characteristics. The texture parameters based on the point cloud calculation are basically the same as the results of the scanning instruments. The process is illustrated in Fig. 4.

In this study, five macro- and micro-texture parameters were calculated based on the point cloud data: macro-MPD, micro-MPD, root mean square height (*Sq*), skewness (*Ssk*), and kurtosis (*Sku*). Additionally. Macro-MPD is the most commonly used indicator for evaluating pavement macrotexture, and numerous studies have shown that changes in macro-MPD are directly related to the friction between tires and pavement. In this study, macro-MPD was calculated in following ISO 13473–1:2019. Data preprocessing was required to standardize the data before MPD calculation. This process involved first removing and correcting invalid points in the raw data, then resampling the point cloud

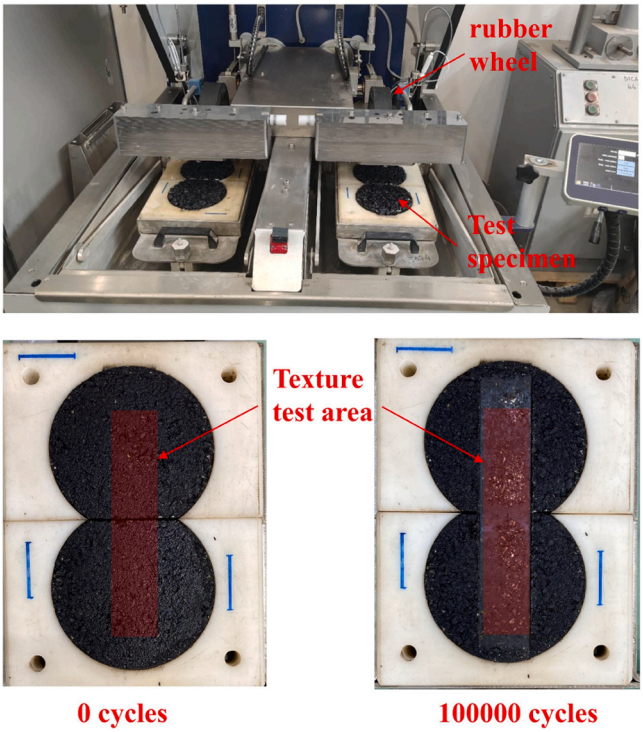

Fig. 6. Schematic diagram of the HWTD and texture test area.

data to meet the specified resolution. Next, spike identification and profile reshaping were applied to the data. High-pass and low-pass filtering were subsequently performed to remove slope and long-wavelength components, while also standardizing sharpness. Once the data was optimized, the mean segment depth (MSD) was calculated, as illustrated in Fig. 5. For this calculation, a 100 mm baseline was divided into two segments, and the MSD was defined as the average of the two peak heights. The macro-MPD for the entire test area was obtained as the average MSD value across all profiles.

Microtexture, with a wavelength $\leq$ 0.5 mm, primarily contributes to the adhesion between tires and pavement and affects skid resistance at low speeds. Currently, there is no standardized method for calculating micro-MPD. Therefore, this study applied the same calculation method as for macrotexture, but adjusted the baseline standard to 1 mm (with each segment length equal to 0.5 mm), as shown in Fig. 5.

In this study, multiple characteristic texture parameters were extracted from the preprocessed 3D texture point cloud data based on the ISO 25178 standard. The area root mean square (Sq) is a texture height parameter used to evaluate the peak and valley magnitude of the macrotexture profile, reflecting the roughness characteristics of the measured area. The calculation formula for Sq is as follows:

$$Sq = \sqrt{\frac{1}{A}\iint_A Z^2(x,y)dxdy} \tag{1}$$

The Ssk value (skewness) indicates texture distribution. $Ssk = 0$ means a symmetric distribution, When $Ssk < 0$, there are more peaks in the texture, with the height distribution skewed below the mean surface level. When $Ssk > 0$, there are more valleys or depressions in the texture, with the height distribution skewed above the mean surface level. The Sku value is used to assess the sharpness in the height distribution, where $Sku = 3$ indicates a normal distribution, $Sku > 3$ signifies a steep height distribution, and $Sku < 3$ suggests a uniform height distribution. The calculation formulas for Ssk and Sku are as follows:

Table 3
Components of bitumen model [35].

Components	Molecules	Molecular representation	Number in model	Molar mass (g/mol))
Saturate	Squalane	$C_{30}H_{62}$	4	422.9
	Hopane	$C_{35}H_{62}$	4	483.0
Aromatic	PHPN	$C_{35}H_{44}$	11	464.8
	DOCHN	$C_{30}H_{46}$	13	406.8
Resin	Quinolinohopane	$C_{40}H_{59}N$	4	554.0
	Thioisorenieratane	$C_{40}H_{60}S$	4	573.1
	Trimethylbenzeneoxane	$C_{29}H_{50}O$	5	414.8
	Pvridinohopane	$C_{36}H_{57}N$	4	530.9
	Benzobisbenzothiophene	$C_{18}H_{10}S_2$	15	290.4
Asphaltene	Asphaltene-phenol	$C_{42}H_{54}O$	3	575.0
	Asphaltene-pyrrole	$C_{66}H_{81}N$	2	888.5
	Asphaltene-thiophene	$C_{51}H_{62}S$	3	707.2

$$Ssk = \frac{1}{Sq^3}\left[\frac{1}{A}\iint_A Z^3(x,y)dxdy\right] \tag{2}$$

$$Sku = \frac{1}{Sq^4}\left[\frac{1}{A}\iint_A Z^4(x,y)dxdy\right] \tag{3}$$

2.2.3. Long-term texture characterization

The study utilized a Hamburg Wheel Tracking Device (HWTD) to simulate changes in pavement texture characteristics over long-term service. The two types, a 47 mm wide rubber wheel and a steel wheel, were used to simulate pavement loading under different conditions. The load on the wheel was 705 $\pm$ 4.5 N, with a maximum speed of approximately 0.305 m/s at the midpoint of the sample. Texture characteristics in the test area were measured after 0–100000 load cycles. The HWTD and texture testing area are shown in Fig. 6. The experiment assessed texture changes in pavement contaminated with various hazardous spills after long-term evolution.

2.2.4. Skid resistance

This study assessed pavement skid resistance using the British Pendulum Tester. The skid resistance and micro-friction of the pavement surface were evaluated by measuring the Pendulum Test Value (PTV) at a single point. Following European Standard EN 13036–4, the British Pendulum Tester was used to measure the British Pendulum Number (BPN) multiple times at the same point, and an average was calculated to obtain the initial PTV. This PTV was then corrected for ambient temperature to yield the final PTV.

2.3. Molecular dynamics simulations

In this study, the primary components of pavement materials are bitumen and aggregates. To effectively simulate the material properties, a molecular model of bitumen was first constructed. Bitumen, as a complex compound, comprises thousands of chemical constituents, making it challenging to precisely define its composition [32,33]. However, bitumen is typically classified into four main components: asphaltenes, resins, aromatics, and saturates. Many studies have established bitumen models based on these four components, and results indicate that such models effectively represent the characteristics of bitumen [34]. This study adopts the twelve-component bitumen model proposed by Li and Greenfield, with details of each component listed in Table 3.

To characterize the properties of aggregates, a single-cell model was utilized in this study. The aggregate materials are mainly basalt and limestone, primarily composed of SiO_2, Al_2O_3, and $CaCO_3$, with SiO_2 content typically exceeding 50 %. Therefore, quartz (SiO_2) was selected as the representative aggregate material for molecular dynamics

Table 4
Components of petrol and diesel.

Components	Molecules	Molecular representation	Mass composition (%)	Molar mass (g/mol))
Petrol	n-hexane	C_6H_{14}	26	86.2
	Thiophene	C_4H_4S	6	84.1
	Isooctane	C_8H_{18}	26	114.2
	Heptane	C_7H_{16}	26	100.2
	Pyridine	C_5H_5N	6	79.1
	Toluene	C_7H_8	10	92.1
Diesel	Thiophene	C_4H_4S	3	84.1
	Heptane	C_7H_{16}	26	100.2
	Pyridine	C_5H_5N	6	79.1
	Toluene	C_7H_8	10	92.1
	n-dodecane	$C_{12}H_{26}$	26	170.3
	n-hexadecane	$C_{16}H_{34}$	26	226.5
	Dibenzothiophene	$C_{12}H_8S$	3	184.3

simulation.

In this study, the molecular models for petrol and diesel were constructed based on Edgar et al.'s investigation of their respective compositions [36]. The details of each component are listed in Table 4. For brake fluid and engine oil, molecular dynamics models were developed using the primary components listed in the specifications. The final molecular models of various hazardous spill substances, as well as the bitumen and aggregate models, are presented in Table 5. The dimensions of the aggregate molecule are 30.39 Å × 37.84 Å × 30.65 Å. The other molecules have the same length and width as the aggregate molecule, with a slight difference in height due to compositional differences.

Fig. 7 depicts the interface model constructed for hazardous spills and bitumen. Since bitumen dissolves in hazardous spills, no positional constraints were applied to the bitumen model. The upper layer consists of contaminant molecules, while the lower layer contains bitumen molecules. This model was geometrically optimized over 10,000 iterations. A vacuum layer of 30 Å was added above the model to prevent

Table 5
Molecular dynamics model.

Molecular model		Schematic	
Types	Bitumen	Aggregate	Diesel
	Petrol	Engine oil	Brake fluid

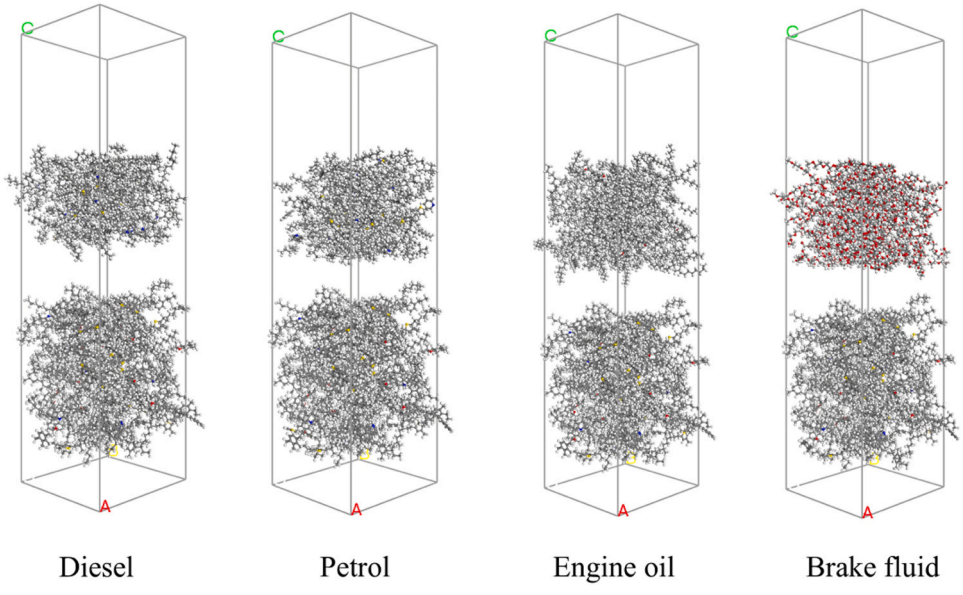

Fig. 7. Molecular modeling of different hazardous spills and bitumen.

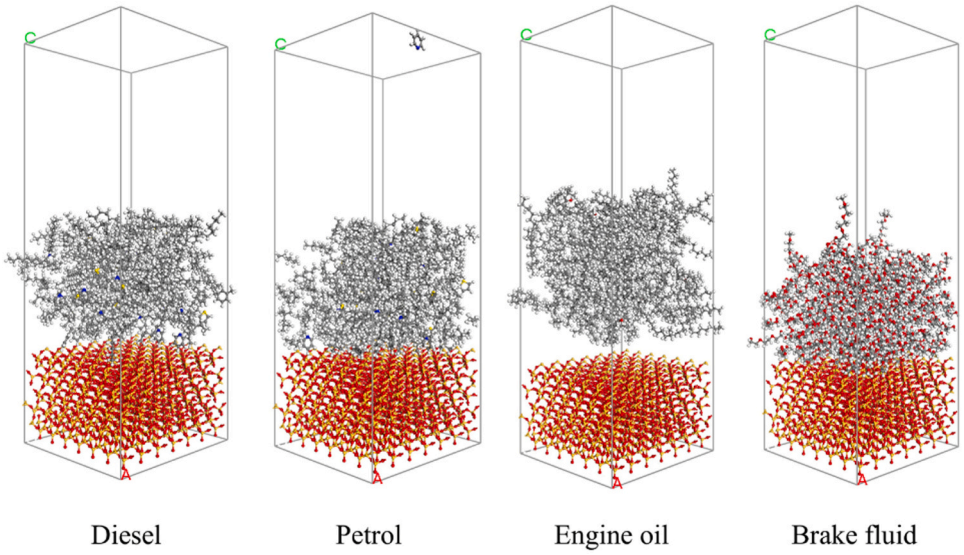

Fig. 8. Molecular modeling of different hazardous spills and aggregates.

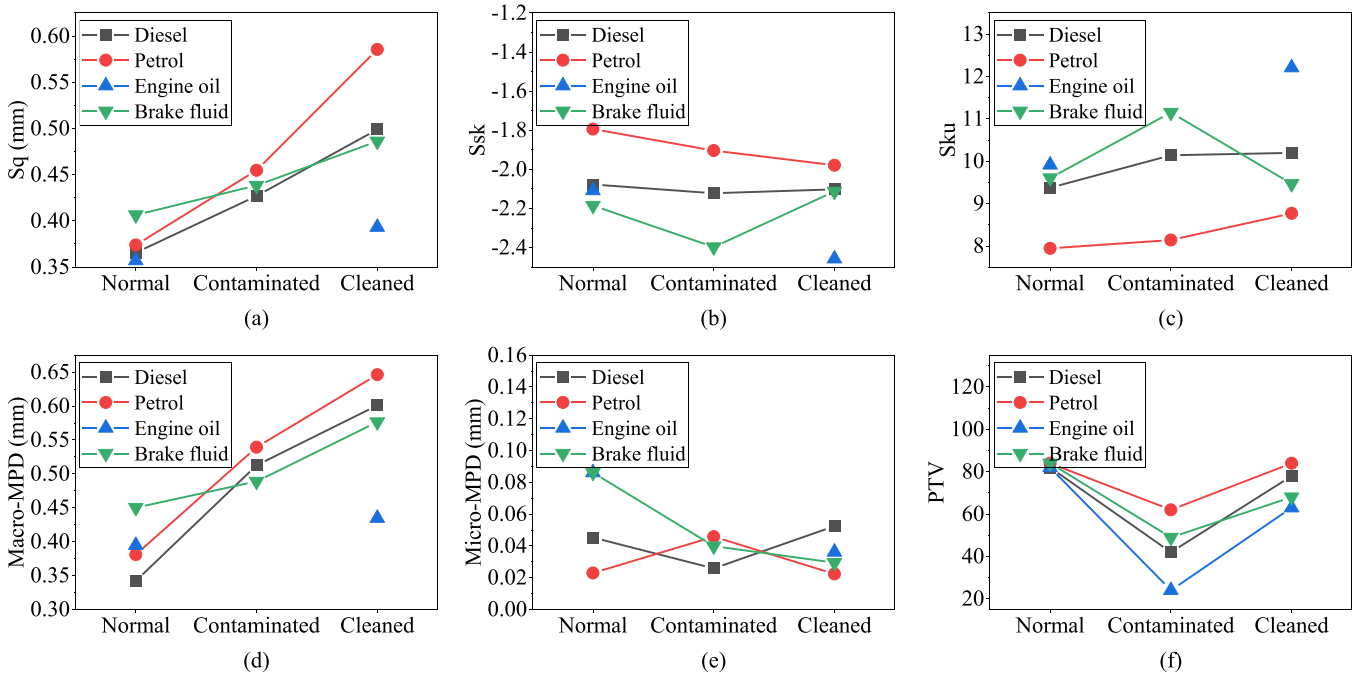

Fig. 9. Results of pavement roughness parameters and skid resistance performance.

cross-image interactions along the z-axis. Fig. 8 illustrates the interface model constructed for hazardous spills and aggregates. As aggregate positions remain unchanged, constraints were applied to the aggregate positions. The aggregate model was created by cleaving a silica unit along the [0, 0, 1] direction, followed by a supercell operation. In this model, the aggregates occupy the lower layer, while the upper layer consists of contaminant molecules. Similar to the bitumen model, this configuration underwent geometric optimization and was supplemented with a 30 Å vacuum layer. Finally, all models were subjected to a 100 ps dynamic equilibrium simulation under a canonical ensemble (NVT). The temperature of the simulation is 300 K.

3. Results and discussions

3.1. Short-term effects of hazardous spills on pavement texture

3.1.1. Effects of contamination on pavement texture

The surface texture parameters and skid resistance results before and after contamination by different contaminants are shown in Fig. 9. Due to the prolonged presence of engine oil on the pavement after contamination, texture measurements could not be conducted, and thus texture data under engine oil contamination is missing. Fig. 9(a)–Fig. 9(c) depict traditional roughness parameters. After contamination and subsequent cleaning of the pavement surface, *Sq* gradually increased, with the most significant increase observed on the petrol-contaminated pavement, rising from 0.38 to 0.59. The *Ssk* value of the pavement surface slightly decreases when contaminated with petrol and engine oil, while it

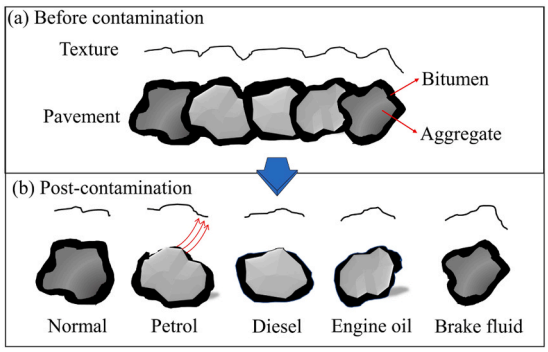

Fig. 10. Change in pavement texture before and after contamination.

fluctuates under diesel and brake fluid contamination. The *Sku* value changes in the opposite direction to *Ssk, but overall, Ssk* and *Sku* showed no obvious trends. Interestingly, the pavement became rougher after contamination and cleaning, which may be attributed to the fact that it was newly paved. This process is similar to the early service stage of pavement, aligning with previous research findings that suggest an initial increase in pavement texture roughness during early service life.

Roughness changes early in service are mainly due to bituminous abrasion, and therefore may be caused by the interaction between bitumen and contamination. Petrol and diesel, composed of various hydrocarbons, are chemically similar to bitumen, which enables good miscibility with bitumen. Smaller hydrocarbon molecules in petrol and diesel (e.g., hexane, heptane) can penetrate bitumen macromolecular structure, promoting diffusion and dissolution. Petrol also dissolves bitumen and, due to its volatility, carries away some bitumen components during evaporation. Engine oil, primarily composed of mineral or synthetic base oils rich in hydrocarbons, has partial miscibility with bitumen. However, due to substantial compositional differences, engine oil and bitumen do not completely dissolve and typically form a mixture. Brake fluid, mainly composed of alcohols and ethers, is largely incompatible with bitumen. The overall miscibility of these four hazardous substances with bitumen ranks as follows: petrol > diesel > engine oil > brake fluid.

Fig. 9(d) – Fig. 9(f) also shows macro-MPD, micro-MPD and skid resistance. Macro-MPD and *Sq* exhibit similar trends. Petrol and diesel cause the most significant changes after contamination and subsequent cleaning. The values increased notably from 0.38 to 0.65 for petrol and from 0.34 to 0.6 for diesel. Micro-MPD shows a similar fluctuation trend as *Ssk* and *Sku*. Prior to contamination, the PTV values of the pavements at different test points were essentially equal because the pavements were of the same type. The PTV value decreased after contamination, with an average reduction of 47 %. Notably, after engine oil contamination, the PTV value dropped by 71 %, posing a severe safety hazard for driving, necessitating immediate treatment. After cleaning, PTV partially recovers, and in the case of petrol and diesel contamination, it even reaches a higher level. This may be due to the bitumen film being dissolved, which increases the contact area with aggregate, enhancing skid resistance and counteracting the contamination effects on skid resistance. Typically, a greater surface profile depth correlates with better skid resistance. After petrol and diesel contamination, slight increases in profile depth may explain the recovery of skid resistance on cleaned surfaces.

Fig. 10 illustrates changes in surface texture following contamination. Since petrol and diesel dissolve bitumen, their presence on the pavement surface affects the bitumen film, which in turn affects the texture wear process and alters the texture. This change is evident in a significant increase in the surface roughness parameter *Sq*. When the surface is contaminated by engine oil or brake fluid, these substances mostly adhere to the surface layer without noticeably affecting the bitumen. After cleaning, any slight loss of bitumen caused by the cleaning process results in minimal changes in roughness, showing little difference compared to the initial surface. The roughness parameters *Ssk* and *Sku* display no clear trends, possibly due to the lack of significant wear on the surface. Since the bitumen film adheres uniformly to the aggregate, any texture changes are uniform in both positive and negative directions, leading only to minor fluctuations in *Ssk* and *Sku*.

3.1.2. Correlation between roughness and skid resistance

Fig. 11 presents the Pearson correlation coefficients for both new pavement surfaces and pavement surfaces subjected to contamination and subsequent cleaning. In addition to the five height parameters analyzed previously, the table also includes functional parameters (*Vm*, *Vv*) and feature parameters (*Spd*, *Spc*) to investigate the correlation between different texture parameters and skid resistance, as well as the interrelationships among texture parameters. *Vm* and *Vv* represent the material and valley volumes per unit area above and below a specific roughness depth, respectively. *Spd* is the number of significant peaks per unit area. *Spc* represents the average curvature of the peaks. As shown in Fig. 11(a), the correlation between roughness parameters and skid resistance (PTV) for normal pavement surfaces is generally weak, with

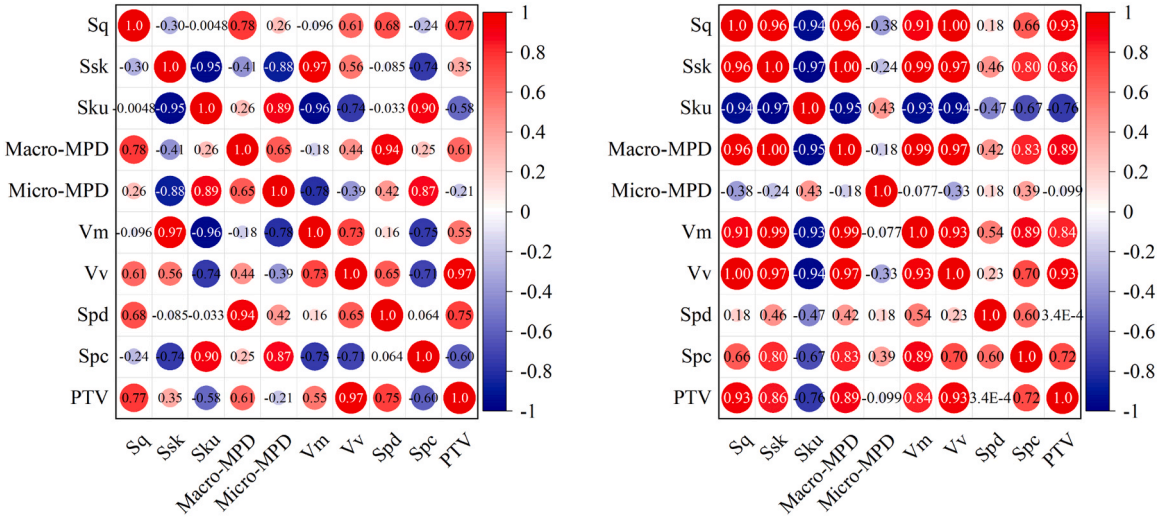

(a) New pavement before contamination (b) Cleaned pavement

Fig. 11. Pearson correlation analysis results.

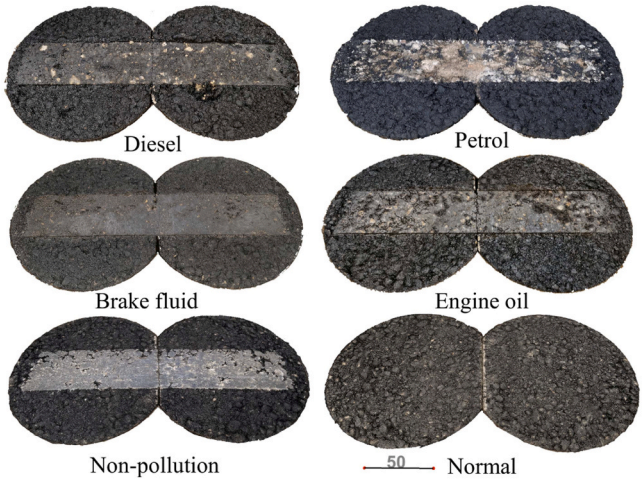

Fig. 12. Metal wheel rutting test.

only *Sq*, *Vv*, and *Spd* exhibiting correlation coefficients greater than 0.7. This finding contradicts many previous studies, which may be attributed to the relatively small variations in roughness among the selected pavement surfaces, all of which are newly constructed.

In contrast, Fig. 11(b) demonstrates a significantly stronger correlation between roughness parameters and skid resistance after the pavement surface has undergone contamination and cleaning. Only Micro-MPD and *Spd* exhibit correlation coefficients below 0.7, indicating that roughness parameters play a more pronounced role in skid resistance. This contrast suggests that, in newly constructed pavement surfaces, the presence of new bitumen covering inhibits the full expression of texture effects, resulting in a weaker correlation between skid resistance and roughness parameters. However, the contamination and cleaning process, is similar to that of allowing a new pavement to serve for a while, during which surface wear exposes texture features more prominently, thereby strengthening the correlation between roughness parameters and skid resistance.

3.2. Long-term effects of hazardous spills on pavement texture

3.2.1. Impact of metal wheel on contaminated pavement surfaces

Fig. 12 illustrates the texture meshes results of specimens subjected

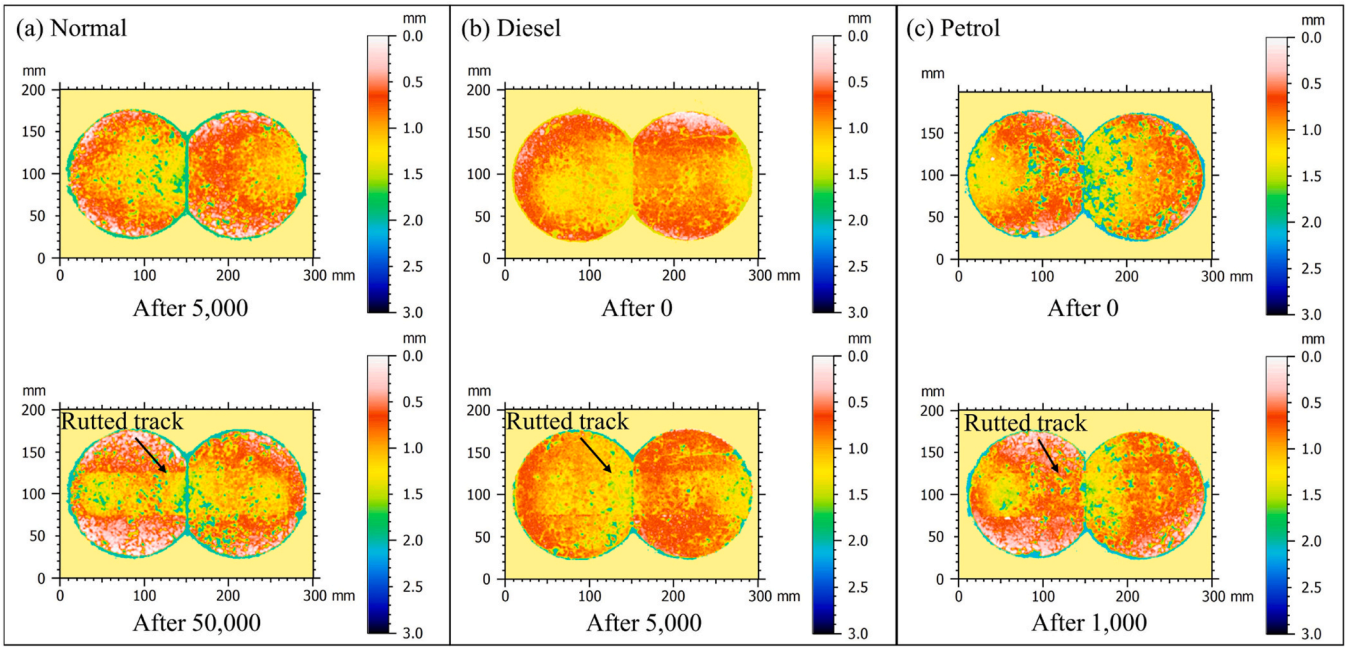

Fig. 13. Rubber wheel rutting test cloud maps.

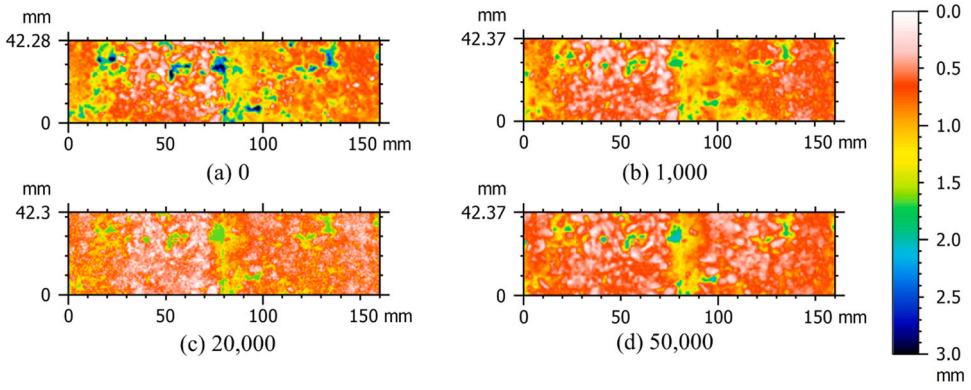

Fig. 14. The petrol-contaminated pavement texture changes under different loading cycles.

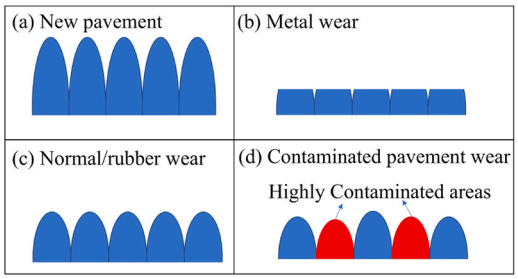

Fig. 15. Diagram of pavement surface abrasion.

to 20000 metal wheel rutting cycles, with tests conducted under different hazardous spills. It should be noted that the normal pavement was not subjected to the rutting test and contaminated process. The results indicate that, regardless of whether the pavement was contaminated, the rutting is visible, and the pavement surface has become nearly flat. Consequently, the roughness parameters of the pavement lose practical significance in this context. However, due to the treatment with different hazardous spill substances, color variations are observed in the wheel track areas. This suggests that contaminants not only interact with the bitumen but also with the aggregates, thereby affecting pavement wear and potentially causing long-term impacts.

3.2.2. *Impact of rubber wheels on contaminated pavement surfaces*

Rutting tests were conducted using rubber wheels on both normal, diesel-contaminated, and petrol-contaminated pavements to evaluate the long-term effects of hazardous spills. The texture cloud map results after rutting tests are shown in Fig. 13. For normal pavements, no rutting marks were observed after 5000 rutting cycles. Noticeable rutting marks appeared only after 50000 cycles. This is primarily due to the elasticity of rubber, which increases the contact area between the rubber wheel and the pavement, reducing localized pressure on the pavement. Consequently, more rutting cycles are required for the rutted track to form. In contrast, on petrol-contaminated pavement, rutting is evident after only 1000 cycles. On diesel-contaminated pavement, rutting was also evident after 5000 cycles. This indicates that contaminants significantly degrade pavement performance, causing rapid texture changes in the wheel track area during loading. The primary reason is that petrol and diesel dissolve the bitumen, weakening the stability of surface aggregates and leading to rapid texture deterioration under repeated loading.

The results of petrol-contaminated pavement texture changes with increasing loading cycles are shown in Fig. 14. It can be observed that the pavement texture changes as the number of loading cycles increases, particularly during the early stages. After 1000 loading cycles, the pavement texture differs significantly from its initial state. However, after a certain degree of wear, the texture tends to stabilize, and further increases in loading cycles result in only minor changes. This indicates that pavements subjected to petrol contamination are more susceptible to wear in the early stages, but the long-term impact is limited, with the texture wear eventually resembling that of uncontaminated pavements.

3.2.3. *Deterioration of texture and skid resistance after pavement contamination*

The deterioration of pavement texture is typically accompanied by a decline in skid resistance. Research has shown that pavement skid resistance decreases rapidly after contamination. However, Claudio et al. [12] found that, over time, the skid resistance of contaminated pavements gradually recovers with prolonged wear and may even exceed pre-contamination levels. This phenomenon is possibly due to uneven wear of pavement aggregates caused by the contamination. The texture deterioration under different pavement conditions is illustrated in Fig. 15. Under normal conditions, pavement texture wears down evenly over time, with aggregates becoming progressively smoother

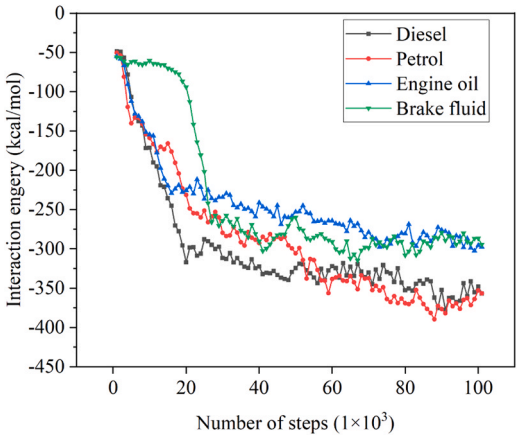

Fig. 16. Interaction energy between hazardous spills and bitumen.

from their initial sharpness. However, when subjected to metal wheel abrasion, the pavement experiences severe damage, and its texture may be completely flattened. Additionally, when exposed to hazardous spills such as petrol or diesel, which can dissolve bitumen, some areas of the bitumen are dissolved or even evaporate. This exacerbates localized damage, causing uneven wear. Paradoxically, this uneven wear can enhance skid resistance in certain areas to some extent.

3.3. *Interaction between bitumen and hazardous spills*

This study is based on the Material Studio simulation software, utilizing the COMPASS force field for interaction between bitumen and hazardous spills. Interactions can be analyzed by adhesion work. Adhesion work refers to the energy required to separate two materials per unit area under vacuum conditions. The adhesion work reflects the adhesive strength between the two materials: the greater the adhesion work, the stronger the adhesive force, and the more difficult it is to separate them. Calculating the adhesion work necessitates an analysis of interaction energy, which requires knowledge of the surface energies of the two individual materials as well as the total energy of the system, as expressed in Eq. (4). The adhesion work can then be determined by dividing the interaction energy by the contact area, as shown in Eq. (5). A positive value of the calculated adhesion work indicates repulsion between the two materials, while a negative value indicates attraction. Consequently, analyzing the interaction energies between various contaminants and bitumen or aggregates can provide insights into the short-term and long-term mechanisms of contaminant effects on pavement performance.

$$\Delta E = E_{total} - (E_1 + E_2) \tag{4}$$

$$W_{adhesion} = \Delta E / A \tag{5}$$

Where ΔE represents the interaction energy, E_{total} denotes the total potential energy at equilibrium when the hazardous spill interacts with bitumen or aggregates, E_1 is the potential energy of the hazardous spill, and E_2 represents the potential energy of bitumen or aggregates. A is the contact area between them, and $W_{adhesion}$ refers to the adhesion work between the two materials.

Fig. 16 illustrates the variation of interaction energy during the dynamic equilibrium process, showing that the system achieves a relatively stable state after approximately 30000 steps. The interaction energy between hazardous spills and bitumen is negative, indicating an attractive force between the two materials. Once hazardous spills are deposited on the bitumen surface, they tend to adhere to it. However, the adhesion strength varies significantly among different contaminants. In terms of the absolute values of interaction energy, the order is as follows: petrol > diesel > brake fluid> engine oil.

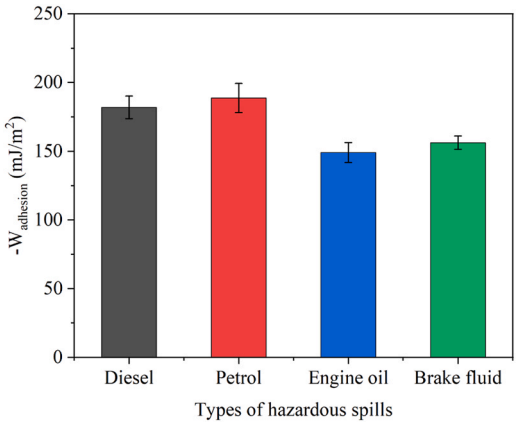

Fig. 17. Work of adhesion between different spills and bitumen.

To further analyze the adhesion strength, the adhesion force per unit area was calculated using data after the 50000th step, as shown in Fig. 17. The results showed that the adhesion between petrol and asphalt was 188.7 mJ/m^2, which is greater than the other hazardous spills. The adhesion between engine oil and bitumen is the smallest, which is only 149.0 mJ/m^2. The brake fluid and the diesel were 156.2 mJ/m^2 and 181.9 mJ/m^2, respectively. This may explain why petrol has the most significant short-term impact on the pavement, with diesel second, while engine oil did not exhibit destructive behavior. Moreover, engine oil showed limited penetration into the pavement or evaporation so it remains on the pavement, making it difficult to collect texture data of the contaminated pavement. This phenomenon is likely attributed to the strong cohesion of engine oil and its weak interaction with bitumen. Therefore, in the case of engine oil contamination, prompt removal is essential; otherwise, it will remain on the pavement for an extended period, posing a high risk of road accidents. Regarding diesel, its solubility is inferior to that of petrol, and its adhesion properties are also relatively low. Consequently, its dissolution reaction with bitumen is significantly reduced.

The molecular schematic after reaching dynamic equilibrium is shown in Fig. 18. Compared to the initial state (Fig. 7), bitumen molecules and various contaminants move closer to each other, exhibiting mutual attraction. This observation aligns with the negative values of interaction energy. By comparing the behavior of the four hazardous spills, it is evident that petrol and diesel differ from engine oil and brake fluid. Specifically, petrol and diesel molecules show a tendency to diffuse outward, indicating that their cohesive forces are insufficient to maintain molecular aggregation. This characteristic corresponds to the inherent volatility of petrol and diesel.

In the case of petrol, some molecules diffuse into the vacuum layer and completely detach from the bitumen molecules. This suggests that, although petrol exhibits a stronger attraction to bitumen than that of the other three substances, some petrol molecules can still volatilize. During this volatilization process, petrol molecules may even carry away small molecular components from the bitumen. This further highlights the short-term adverse effects of petrol spills on bitumen surfaces. In contrast, engine oil and brake fluid, despite having relatively lower interaction energies with bitumen, tend to remain stable above the bitumen surface. This indicates a more stable adhesion behavior due to higher self-cohesion compared to petrol and diesel.

3.4. Interaction between aggregate and hazardous spills

Fig. 19 illustrates the variation in interaction energy during the dynamic equilibrium process between aggregates and different hazardous spills. There are significant differences in the interaction energy between different hazardous spills. The interaction energy between brake fluid and aggregates is the highest, followed by petrol, diesel, and engine oil. This indicates that brake fluid forms stronger adhesion with aggregates and may even penetrate the aggregate structure, potentially influencing its mechanical properties. Fig. 11 also proves this point, where the loaded area of the brake fluid shows the most obvious color change, with the aggregate color completely altered. Although the interaction energy between engine oil and aggregates is relatively low, it is still higher than that between bitumen and hazardous spills, suggesting that aggregates have a stronger adsorption capacity for hazardous spills compared to

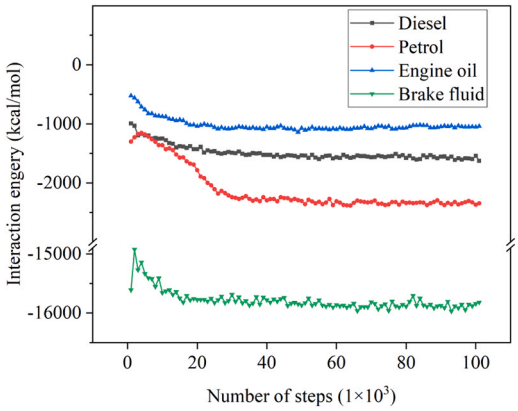

Fig. 19. Interaction energy between hazardous different spills and aggregate.

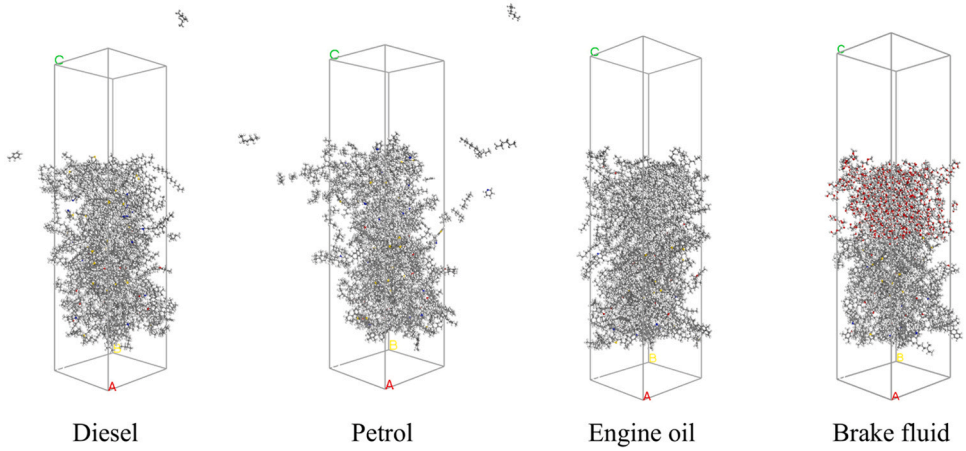

Fig. 18. Schematic diagram of the molecular model after dynamic equilibrium between different spills and bitumen.

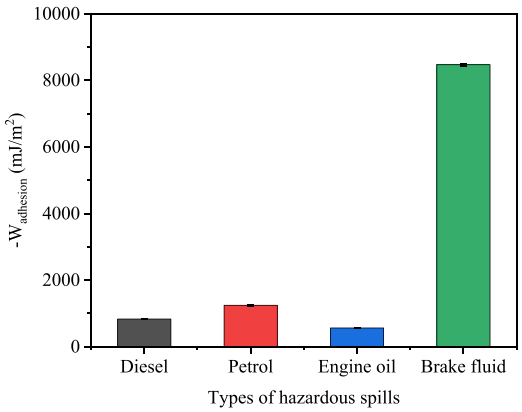

Fig. 20. Work of adhesion between different spills and aggregate.

bitumen. This is mainly because bitumen is a non-polar organic mixture, not easy to adsorb with other substances, while the aggregate surface contains a large number of polar groups. This makes the aggregate easy to absorb with liquids, especially liquids containing polar molecules.

To further compare the adhesion strength, the adhesion force per unit area was calculated based on data obtained after 50000 simulation steps. The results are presented in Fig. 20. The adhesion force between brake fluid and aggregates was found to be 8473.4 mJ/m^2, far exceeding that of other hazardous spills. Petrol ranked second, with an adhesion force of only 1248 J/m^2. This significant difference may be attributed to the high polarity of brake fluid, which contains polyols and esters. These polar molecules form strong hydrogen bonds with the silanol groups on the silica surface, resulting in much stronger adhesion compared to other substances. In contrast, the other three hazardous spills either lack or contain only small amounts of polar molecules, leading to significantly weaker interaction forces. It is worth noting that the polyols in brake fluid are highly hygroscopic and can absorb moisture from the air. When brake fluid penetrates aggregates, it may increase the water content within the aggregate, potentially affecting its mechanical properties and compromising the long-term performance of asphalt pavements.

The molecular structure of aggregates and hazardous spills after reaching dynamic equilibrium is illustrated in Fig. 21. Compared to the initial state (Fig. 8), noticeable changes are observed. In particular, petrol and diesel molecules exhibit significant diffusion of small molecular components into the vacuum layer. This phenomenon is especially pronounced for petrol, where approximately half of its molecules diffuse into the vacuum layer. However, the diffused small petrol molecules are not uniformly distributed within the vacuum layer, all at the top. This non-uniformity arises from the periodic nature of molecular structures modeled in Materials Studio, where diffused molecules are effectively adsorbed onto the top surface of another silica molecule located above the vacuum layer. This adsorption highlights the ease with which these components diffuse, and in real conditions, their high volatility. Petrol components are highly volatile and, during the diffusion process, may carry away small molecular components from the bitumen, causing damage to the pavement surface. In contrast, brake fluid exhibits strong adhesion to the aggregates, with its molecules completely adsorbed onto the aggregate surface. In practical scenarios, a significant portion of brake fluid molecules may infiltrate the aggregates, potentially altering their mechanical properties and impacting the overall performance of the material.

4. Conclusions

This study investigates the short-term and long-term effects of various hazardous spills (petrol, diesel, engine oil, and brake fluid) on road pavement performance. The analysis focuses on changes in skid resistance and surface texture parameters following contamination and subsequent cleaning procedures. In addition, the interactions between bitumen and each pollutant were evaluated through molecular dynamics (MD) simulations to better understand the mechanisms underlying pavement deterioration. Each contaminant exhibits distinct impacts on pavement characteristics. Petrol and diesel tend to dissolve bitumen, thereby accelerating long-term damage. In contrast, oily substances such as engine oil and brake fluid remain on the surface, compromising road safety by reducing tire–pavement friction. The key findings of the study can be summarized as follows:

- Engine oil results in the greatest reduction in skid resistance when not removed. While cleaning procedures tend to restore skid performance, they are not fully effective in the case of oily substances, which can infiltrate asphalt concrete and resurface under traffic loading. Conversely, in the case of hydrocarbon spills such as petrol and diesel, the partial dissolution of surface bitumen may temporarily improve skid resistance due to increased microtexture exposure.
- Petrol significantly weakens the bond between bitumen and aggregates, leading to rutting deformation under shorter loading durations. Diesel and engine oil produce similar effects, though with comparatively less severity. Brake fluid, however, does not appear to contribute substantially to mechanical deformation.
- The molecular dynamics simulations reflect experimental observations. Petrol exhibits a strong binding affinity to bitumen but volatilizes quickly, causing material loss and short-term surface damage. Diesel behaves similarly but with lower volatility. Engine oil interacts weakly with bitumen yet remains persistent on the surface, while brake fluid shows strong adhesion to aggregates, which may potentially compromise their structural stability.

As the results have demonstrated, different hazardous substances

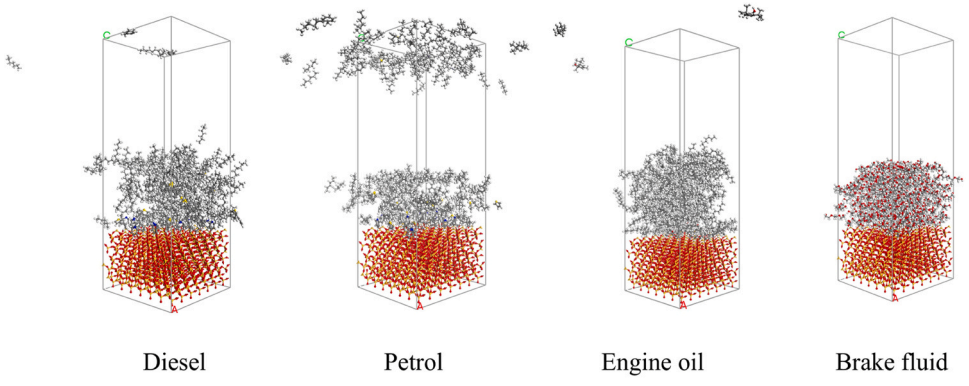

Fig. 21. Schematic diagram of the molecular model after dynamic equilibrium between different spills and aggregate.

pose distinct threats to road pavements, compromising user safety and significantly influencing maintenance strategies for road authorities. This study contributes to a deeper understanding of how various contaminants interact with asphalt concrete, identifying which pavement properties are most affected in both the short and long term.

Future research will explore the behavior of high-performance pavement materials, such as mixtures based on polymer-modified bitumen (PmB) or recycled asphalt pavement (RAP), uder similar contamination scenarios. Additionally, investigations will be extended to assess the effects of non-liquid or composite pollutants, including snow, ice, slush, and dust, to enhance the overall understanding of how diverse environmental contaminants influence road surface performance and durability.

CRediT authorship contribution statement

Zhenlong Gong: Writing – original draft, Methodology, Investigation, Conceptualization. **Marco Bruno:** Writing – original draft, Formal analysis, Data curation. **Claudio Lantieri:** Supervision, Investigation, Data curation. **Margherita Pazzini:** Writing – review & editing, Validation, Methodology. **Yinghao Miao:** Writing – review & editing, Supervision.

Declaration of Competing Interest

The authors declare that they have no known competing financial interests or personal relationships that could have appeared to influence the work reported in this paper.

Acknowledgments

This study was carried out within the Spoke 7 of the MOST—Sustainable Mobility National Research Center and received funding from the EUROPEAN UNION Next-Generation EU (PIANO NAZIONALE DI RIPRESA E RESILIENZA (PNRR)—MISSIONE 4 COMPONENTE 2, INVESTIMENTO 1.4—D.D. 1033 17/06/2022, CN00000023). This manuscript reflects only the authors' views and opinions. Neither the European Union nor the European Commission can be considered responsible for them.

This work was also supported by China Scholarship Council (No. 202306460065).

Data Availability

The data that has been used is confidential.

References

[1] P. Bertoli, V. Grembi, The political cycle of road traffic accidents, J. Health Econ. 76 (2021) 102435, https://doi.org/10.1016/j.jhealeco.2021.102435.
[2] R. Kmet, Z. Dvorak, M. Kvet, Map of traffic accidents, Transp. Res. Procedia 40 (2019) 1418–1425, https://doi.org/10.1016/j.trpro.2019.07.196.
[3] P. Sadeghi, A. Goli, Investigating the impact of pavement condition and weather characteristics on road accidents (review paper), Int. J. Crashworthiness 29 (6) (2024) 973–989, https://doi.org/10.1080/13588265.2024.2348269.
[4] H.L. Dai, K.L. Zhang, X.L. Xu, H.Y. Yu, Evaluation on the effects of deicing chemicals on soil and water environment, Procedia Environ. Sci. 13 (2012) 2122–2130, https://doi.org/10.1016/j.proenv.2012.01.201.
[5] J.M. Pardillo Mayora, R. Jurado Piña, An assessment of the skid resistance effect on traffic safety under wet-pavement conditions, Accid. Anal. Prev. 41 (4) (2009) 881–886, https://doi.org/10.1016/j.aap.2009.05.004.
[6] S.K. Ahmed, M.G. Mohammed, S.O. Abdulqadir, R.G.A. El Kader, N.A. El Shall, D. Chandran, M.E.U. Rehman, K. Dhama, Road traffic accidental injuries and deaths: a neglected global health issue, Health Sci. Rep. 6 (5) (2023) e1240, https://doi.org/10.1002/hsr2.1240.
[7] D. Yang, K. Peng, J. Zheng, B. Xie, J. Wang, B. Xu, F. Li, Consequences analysis of the LPG tank truck traffic accident: a case study of the wenling explosion accident, J. Loss Prev. Process Ind. 87 (2024) 105228, https://doi.org/10.1016/j.jlp.2023.105228.
[8] O. Simsekoglu, T. Nordfjaern, The role of safety culture/climate and social cognitive factors for driving behaviors of turkish professional drivers transporting petroleum products, J. Risk Res 20 (5) (2017) 650–663, https://doi.org/10.1080/13669877.2015.1118150.
[9] B. Adrià Mora, M. Hilpert, Differences in infiltration and evaporation of diesel and gasoline droplets spilled onto concrete pavement, Sustainability 9 (7) (2017) 1271, https://doi.org/10.3390/su9071271.
[10] V.A. Girelli, L. Cotignoli, N. Ghasemi, C. Lantieri, M.A. Tini, R. Vecchione, G. Bitelli, V. Vignali, Assessing hazardous spills impact on road surface performances by 3d high resolution surveying techniques. in, Springer International Publishing, Cham, 2023, pp. 265–279.
[11] T. Tsubota, C. Fernando, T. Yoshii, H. Shirayanagi, Effect of road pavement types and ages on traffic accident risks, Transp. Res. Procedia 34 (2018) 211–218, https://doi.org/10.1016/j.trpro.2018.11.034.
[12] C. Lantieri, N. Ghasemi, L. Cotignoli, V. Vignali, A. Simone, The evaluation of the effects of hazardous spills by road accidents on the surface performance of an asphalt-wearing course, Int J. Pavement Eng. 24 (2) (2023) 1–13, https://doi.org/10.1080/10298436.2022.2138878.
[13] P. Chaturabong, T.T. Lim, Y.D. Wong, Effective surface treatment techniques for refinishing oil-stained road surface, Constr. Build. Mater. 159 (2018) 64–72, https://doi.org/10.1016/j.conbuildmat.2017.10.082.
[14] X. Wang, Y. Huang, L. Geng, M. Li, H. Han, K. Li, Q. Xu, Y. Ding, T. Zhang, Multiscale performance of composite modified cold patch asphalt mixture for pothole repair, Constr. Build. Mater. 371 (2023) 130729, https://doi.org/10.1016/j.conbuildmat.2023.130729.
[15] C. Wang, M. Wang, X. Xiao, J. Guo, Preparation and evaluation of durability of color antiskid pavement particles subjected to different treatments, J. Mater. Civ. Eng. 32 (1) (2020) 4019336, https://doi.org/10.1061/(ASCE)MT.1943-5533.0002992.
[16] B.N.J. Persson, Theory of rubber friction and contact mechanics, J. Chem. Phys. 115 (8) (2001) 3840–3861, https://doi.org/10.1063/1.1388626.
[17] P. Cui, S. Wu, Y. Xiao, C. Yang, F. Wang, Enhancement mechanism of skid resistance in preventive maintenance of asphalt pavement by steel slag based on micro-surfacing, Constr. Build. Mater. 239 (2020) 117870, https://doi.org/10.1016/j.conbuildmat.2019.117870.
[18] W. Zhao, J. Zhang, J. Lai, X. Shi, Z. Xu, Skid resistance of cement concrete pavement in highway tunnel: a review, Constr. Build. Mater. 406 (2023) 133235, https://doi.org/10.1016/j.conbuildmat.2023.133235.
[19] S. Chen, X. Liu, H. Luo, J. Yu, F. Chen, Y. Zhang, T. Ma, X. Huang, A state-of-the-art review of asphalt pavement surface texture and its measurement techniques, J. Road. Eng. 2 (2) (2022) 156–180, https://doi.org/10.1016/j.jreng.2022.05.003.
[20] F. Guo, J. Pei, J. Zhang, R. Li, B. Zhou, Z. Chen, Study on the skid resistance of asphalt pavement: a state-of-the-art review and future prospective, Constr. Build. Mater. 303 (2021) 124411, https://doi.org/10.1016/j.conbuildmat.2021.124411.
[21] T.F. Fwa, L. Chu, The concept of pavement skid resistance state, Road. Mater. Pavement Des. 22 (1) (2021) 101–120, https://doi.org/10.1080/14680629.2019.1618366.
[22] D. Chen, X. Yang, M. Zhong, C. Chen, L. Wang, J. Wang, X. Weng, Y. Li, Z. Chang, Inspired by tree frog: bionic design of tread pattern and its wet friction properties, J. Bionic Eng. 19 (4) (2022) 1064–1076, https://doi.org/10.1007/s42235-022-00184-2.
[23] T.F. Fwa, S.S. Kumar, K. Anupam, G.P. Ong, Effectiveness of tire-tread patterns in reducing the risk of hydroplaning, Transp. Res Rec. 2094 (1) (2009) 91–102, https://doi.org/10.3141/2094-10.
[24] Y. Miao, P. Song, X. Gong, Fractal and multifractal characteristics of 3d asphalt pavement macrotexture, J. Mater. Civ. Eng. 26 (8) (2014) 4014033, https://doi.org/10.1061/(ASCE)MT.1943-5533.0000912.
[25] P. Cui, T. Ma, S. Wu, G. Xu, F. Wang, Texture characteristic and its enhancement mechanism in stone mastic asphalt incorporating steel slag, Constr. Build. Mater. 369 (2023) 130440, https://doi.org/10.1016/j.conbuildmat.2023.130440.
[26] X. Huan, Y. Sheng, L. Wang, Z. Ye, L. Li, H. Xue, Y. Zhang, H. Zhao, Evolution of texture and skid resistance change of high-friction surface due to differential-polishing undergoing simulated traffic wear, Tribol. Int 177 (2023) 107944, https://doi.org/10.1016/j.triboint.2022.107944.
[27] A.P. Pérez-Fortes, M.J. Varas-Muriel, P. Castiñeiras, Long-term behavior of the micro-texture of aggregates used on roads subjected to extreme climate conditions and winter maintenance operations, Wear 474-475 (2021) 203757, https://doi.org/10.1016/j.wear.2021.203757.
[28] J. Gerthoffert, V. Cerezo, M. Bouteldja, M. Do, Modeling aircraft braking performance on wet and snow/ice-contaminated runways, Proc. Inst. Mech. Eng. Part J. J. Eng. Tribol. 229 (9) (2015) 1065–1078, https://doi.org/10.1177/1350650115572450.
[29] Y. Hichri, V. Cerezo, M.T. Do, Modeling of the surface coverage and application to the calculation of friction on surfaces contaminated by particles, Wear 426-427 (2019) 1082–1093, https://doi.org/10.1016/j.wear.2018.12.086.
[30] M. Bruno, V. Vignali, A. Simone, C. Lantieri, A laboratory and field recovery estimation of cleaned road surfaces after accidents spills contamination and traffic simulation, Road. Mater. Pavement Des. (2025) 1–19, https://doi.org/10.1080/14680629.2025.2485334.
[31] Z. Gong, M. Bruno, M. Pazzini, A. Forte, V.A. Girelli, V. Vignali, C. Lantieri, Low-cost and contactless survey technique for rapid pavement texture assessment using mobile phone imagery, Sustainability 16 (22) (2024) 9630, https://doi.org/10.3390/su16229630.
[32] H. Zhang, F. Zheng, J. Zhang, D. Hu, X. Yu, Z. Chen, J. Pei, Unveiling micro-macro links in asphalt: an in-depth analysis of characterization and simulation approaches, Fuel (Lond.) 379 (2025) 132823, https://doi.org/10.1016/j.fuel.2024.132823.

[33] D.D. Li, M.L. Greenfield, Viscosity, relaxation time, and dynamics within a model asphalt of larger molecules, J. Chem. Phys. 140 (3) (2014) 34507, https://doi.org/10.1063/1.4848736.
[34] G. Xu, H. Wang, Molecular dynamics study of interfacial mechanical behavior between asphalt binder and mineral aggregate, Constr. Build. Mater. 121 (2016) 246–254, https://doi.org/10.1016/j.conbuildmat.2016.05.167.
[35] D.D. Li, M.L. Greenfield, Chemical compositions of improved model asphalt systems for molecular simulations, Fuel (Lond.) 115 (2014) 347–356, https://doi.org/10.1016/j.fuel.2013.07.012.
[36] E. Núñez-Rojas, K.G. Alarcón, J. Alejandre, Extraction of n- and s-compounds in gasoline and diesel from ionic liquids: a molecular dynamics study, J. Mol. Liq. 397 (2024) 124102, https://doi.org/10.1016/j.molliq.2024.124102.